Frequency-dependent wave velocities in sediments and sedimentary rocks: Laboratory measurements and evidences

Andreas Bauer[1, 2], Mohammad Hossain Bhuiyan[1], Erling Fjær[1, 2], Rune M. Holt[2], Serhii Lozovyi[2], Mathias Pohl[3], and Dawid Szewczyk[2]

Abstract

The pioneering work of Mike Batzle and his colleagues has provided a fundamental understanding of mechanisms behind dispersion and attenuation of elastic waves in fluid-saturated rocks. It also has made way for a realization that these phenomena need to be accounted for in a better way when interpreting seismic and sonic data from the field. Laboratory experiments have formed the basis for new insight in the past and will continue to do so. Here, examples of experimental observations that give direct or indirect evidence for dispersion in sand, sandstone, and shale are presented. Ultrasonic data from compaction tests show that Biot flow is the most likely dispersion mechanism in pure unconsolidated sand. Strong shale dispersion has been identified through low-frequency and low-strain quasistatic measurements and through a novel technique based on static loading and unloading measurements. In shale and sandstone containing clay, there is evidence for water weakening. A comparative study shows an example where the stress dependences of P- and S-wave velocities at seismic frequencies exceed those measured by traditional ultrasonic methods.

Introduction

Velocities in fluid-saturated sedimentary rocks are frequency dependent. In fact, this dispersion is caused largely by the presence of liquids in the pore space (Batzle et al., 2006). Various dispersion mechanisms have been formulated that relate to wave-induced fluid flow, either global viscous flow (Biot, 1956), local flow on the pore scale (e.g., O'Connell and Budiansky, 1977), or flow on the mesoscopic scale between patches of different saturations or different permeabilities (e.g., Müller et al., 2010). The transition frequencies span a wide range, depending on the mechanism and on rock and fluid properties. Through the causality principle, dispersion is coupled to wave-energy absorption so that a frequency-dependent velocity implies nonzero absorption (with an absorption peak near the transition frequency) and vice versa.

It is difficult to obtain reliable dispersion from field data. Seismic waves span only one to two orders of frequency magnitudes and are strongly influenced further by heterogeneities at different length scales, so, at most, one may identify traces of frequency dependence. Comparing with vertical seismic profiling (VSP) and sonic log data gives additional information into the 1–10 kHz range, but, again, heterogeneities play a role as does anisotropy. In the laboratory, standard measurements are made by ultrasonic pulse transmission in cm scale core samples. The sample needs to be long enough, or the frequency needs to be high enough, for the sample to accommodate a number of wavelengths. The frequency is limited upward by attenuation (including absorption and scattering by grains and pores), so, in practice, such measurements are only done over a decade or less of frequencies, in the MHz region. Sonic frequencies are rarely addressed in laboratory experiments. Resonance-frequency measurement techniques are employed, requiring long samples. With the split-Hopkinson bar technique (Nakagawa and Kneafsey, 2010), resonance frequencies are measured with smaller rock samples extended by solid rods and inverted for elastic properties of the rock. Again, data are recorded only at one frequency.

In recent years, largely driven by the work performed by Mike Batzle and his colleagues (Batzle et al., 2006), the seismic frequency region has been explored in quasistatic laboratory experiments with very small ($< 10^{-6}$–10^{-7}) strain amplitudes (Spencer, 1981). This technique permits measurements on small samples under stress, pore pressure, and temperature, and may span over several decades of frequency (from 10^{-1} Hz to kHz). Thus, it may reveal fundamental dispersion behavior, particularly when combined with sonic and ultrasonic techniques. Of course, it is limited by sample size, but for understanding of physical phenomena, being able to use the same sample for both ultrasonic propagation and seismic frequency excitation is a clear benefit.

In this paper, we give examples of laboratory measurements that show evidence for dispersion in sediments and sedimentary rocks. We start by showing ultrasonic data that point to Biot dispersion as a main mechanism in unconsolidated sand. We then proceed to show how finite-strain amplitude data acquired in a standard compaction experiment with load-unload cycles may be used to obtain low-frequency elastic stiffnesses. Finally, we show examples of experiments performed in a newly established low-frequency apparatus (Szewczyk et al., personal communication, 2016), based on the principles outlined by Spencer (1981) and Batzle et al. (2006). Here, the impact of fluid saturation on shale dispersion is illustrated, along with a comparison between ultrasonic and seismic frequency stress dependence in a shale sample. A sandstone sample is also included to demonstrate the effect of drained-undrained behavior.

Experimental observations

Uncemented sand: Evidence for Biot dispersion. A common statement in rock physics is that dispersion in cemented sandstone is due to local squirt flow between soft low-aspect pores (pore throats or microcracks) and stiff high-aspect-ratio pores. This statement is validated by several experimental observations (e.g., Mavko and Jizba, 1994). A direct consequence is that increasing stress, leading to closure of soft pores, leads to reduced dispersion. In uncemented sand, microcracks may be found as small gaps within grain contact areas. Xu and White (1995) argue that the average aspect ratio in sand should be around 0.1, which would push the transition frequency for squirt flow into the GHz region, well above frequencies attainable by laboratory measurements. Unconsolidated

[1]SINTEF Petroleum Research.
[2]Norwegian University of Science and Technology.
[3]Colorado School of Mines.

sand, therefore, is expected to exhibit primarily Biot type of dispersion, but this has not been demonstrated in the literature.

Biot dispersion is due to viscous and inertia effects. The transition frequency f_c between low and frequency behavior is:

$$f_c = \frac{\eta\phi}{2\pi k\rho_f}, \tag{1}$$

where η is fluid viscosity, ϕ is porosity, k is permeability, and ρ_f is pore fluid density. For compacted brine-saturated unconsolidated sand, porosity is 35–38%, the permeability is in the range of several Darcy, and hence the transition frequency is typically between 10 and 30 kHz.

From Biot's theory, it follows that the ratio between S-wave velocities in the high-frequency and low-frequency limits is governed entirely by inertia effects:

$$\frac{v_S(f\to\infty)}{v_S(f=0)} = \frac{1}{\sqrt{1-\frac{\phi\rho_f}{T\rho}}}, \tag{2}$$

where ρ is rock bulk density, ρ_f is pore fluid density, and T is a tortuosity factor (a number of the order 1.5–3). This relation is independent of the frame stiffness, which means it is valid at all stresses. In the case of a granular medium close to the suspension limit (Johnson and Plona, 1982), the corresponding ratio between the high- and low-frequency P-wave velocities can be approximated by:

$$\frac{v_P(f\to\infty)}{v_P(f=0)} = \sqrt{\frac{1+\frac{\phi}{T}\left(\frac{\rho}{\rho_f}-2\right)\frac{M_R}{H}}{1-\frac{\phi\rho_f}{T\rho}}}, \tag{3}$$

where M_R is the Reuss average of fluid and solid bulk moduli, and H is the plane wave modulus $\sim K_{fr} + 4/3\, G_{fr} + M_R$. With increasing framework bulk and shear stiffnesses — i.e. with increasing stress on a fluid-saturated granular medium — the resulting P-wave dispersion will decrease. Hence, according to Biot, the stress dependences of P- and S-wave dispersions in a loaded grain pack should show different trends.

Experimental data illustrating this are shown in Figure 1. Columbia Sand was compacted in an oedometer in dry and water-saturated conditions. Ultrasonic velocities (at frequencies ~400 kHz for P-waves and ~130 kHz for S-waves) measured in the water-saturated sand are shown versus net axial stress. In addition, velocities predicted from the low-frequency Gassmann and the high-frequency Biot equations, both based on measurements of the same sand under dry conditions, are compared to the measured data (for further details, see Bhuiyan and Holt, 2016). The high-frequency calculations are made with an anticipated tortuosity factor of 1.7 that remains constant during loading, which gives the best fit to the data. Change in porosity with stress is estimated from the axial and radial strain measurements. Figure 1 confirms the increase in difference between high- and low-frequency S-wave velocities and the decrease in difference between high- and low-frequency P-wave velocities with increasing net stress, as predicted by Biot. Further theoretical adjustments are required to honor the anisotropic nature of the wave propagation in this experiment and possibly also the role of finite frequencies. Further experimental work should be done with saturating fluids having different viscosities and with independent measurements of tortuosity factor by, e.g., electrical resistivity.

Sandstones/shale: Dispersion derived from quasistatic data. Rock stiffness, which is a key parameter controlling wave velocities, can also be measured directly as the slope of the stress-strain relation in a static test. Hence there is a potential for estimating dispersion by comparing static measurements to ultrasonic wave velocities. A number of factors — strain amplitude, saturation, anisotropy, and relevant rock volume — complicate such a procedure. However, careful design of the tests may eliminate all of these complications except strain amplitude. Moreover, Fjær et al. (2013) showed that even the strain-amplitude effect can be eliminated at specific points of a stress path. During unloading, the difference between static and dynamic compliance tends to increase linearly with stress amplitude, allowing for simple extrapolation toward the start of the unloading path. The static compliance at the endpoint of this extrapolation corresponds to the compliance at zero-strain amplitude, and the gap between the static and dynamic uniaxial-strain compliance at this point is a measure of the dispersion in the range from the frequency of the elastic wave to the frequency corresponding to the strain rate of the static measurement. This method for estimation of dispersion requires careful test condition design and good-quality data, but no special equipment beyond what is standard for rock mechanical tests with integrated ultrasonic measurements is required (Fjær et al., 2013).

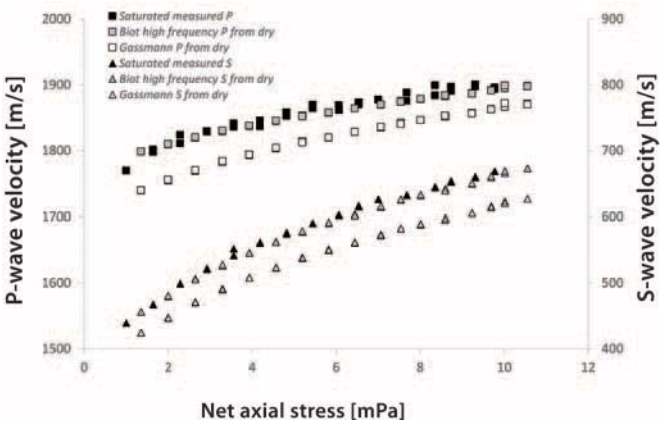

Figure 1. Ultrasonic P-wave (left y-axis) and S-wave (right y-axis) velocities measured versus net axial stress in an oedometer test with brine-saturated Columbia Sand. The sand was dried in an oven overnight at 110°C and then exposed to room humidity before dry velocities were measured during two axial load cycles. The dry data obtained in the second load cycle were used to calculate the saturated velocities according to Gassmann substitution and Biot's high-frequency theory, using a tortuosity factor of 1.7. The saturated velocities were measured during a new load cycle in the same test, with an applied pore pressure of 0.5 MPa.

Using the new low-frequency apparatus at SINTEF (Szewczyk et al., personal communication, 2016), the method proposed by Fjær et al. (2013) was tested and validated for Pierre shale. In Figure 2, we show results obtained with undrained Pierre shale. The quasistatic Young's modulus was obtained from the average slope of the stress-strain curve measured under undrained triaxial unloading. In the present experiment, we obtained E_{static} = 5.5 GPa. As seen in Figure 2b, the compliance, i.e., the tangential slope of the stress-strain curve, $d\varepsilon_{ax}/d\sigma_{ax}$, exhibits a linear dependence on unloading stress, $\Delta\sigma_{ax}$, and can be extrapolated to zero stress. The zero-strain limit of Young's modulus is given by $E_{zero\text{-}strain} = [d\varepsilon_{ax}/d\sigma_{ax}(\Delta\sigma_{ax} = 0)]^{-1}$ = 6.9 GPa. Since the strain rate during unloading corresponds approximately to that of an elastic wave with frequency of about 1 Hz, according to the model by Fjær et al. (2013), $E_{zero\text{-}strain}$ should be close to the dynamic Young's modulus at 1 Hz. This is confirmed by the low-frequency measurements (see Figure 2a), which confirm that dynamic stiffness can be obtained from quasistatic measurements.

Also seen in Figure 2a is a relatively large dispersion of Young's modulus. Between 1 Hz and 500 kHz, Young's modulus increases by about 2.5 GPa, or 36%. Such a large dispersion in Young's modulus is not unusual for shales (Suarez-Rivera et al., 2001; Duranti et al., 2005). For sandstones, dispersion in dynamic stiffness is usually much smaller. It should be noted that in the present experiment, Young's modulus was measured perpendicular to bedding. The ultrasonic Young's modulus was derived from V_S and V_P measured perpendicular to bedding by assuming Thomsen anisotropy parameters obtained from different Pierre-shale experiments under similar stress conditions (ε = 0.13; γ = 0.25; δ = 0.10).

Sandstones: Water-induced rock softening. In the above example with synthetic unconsolidated sand (see Figure 1), ultrasonic velocities of dry and water-saturated samples could well be described by assuming the matrix stiffness is not affected by the water. For natural rocks, this assumption is often not valid; interaction with water often results in significant rock softening (Khazanehdari and Sothcott, 2003; Adam et al., 2006). The underlying mechanisms are not fully understood yet. Here, we show results for Fox Hill sandstone (porosity of about 29%, mostly quartz, some clay). The experiments were carried out in the low-frequency apparatus referenced above (Szewczyk et al., personal communication, 2016) with two different samples. Figure 3 shows the dynamic undrained Young's modulus and the undrained Poisson's ratio as a function of frequency. The samples were first measured under dry conditions (open symbols in Figure 3). Subsequently, sample no. 1 was saturated with oil, and sample no. 2 was saturated with water. Oil saturation results in an increase in both Young's modulus and Poisson's ratio. The increase in Poisson's ratio is in agreement with Gassmann's fluid-substitution theory; the measured increase in Young's modulus, however, is smaller than expected by the Gassmann model.

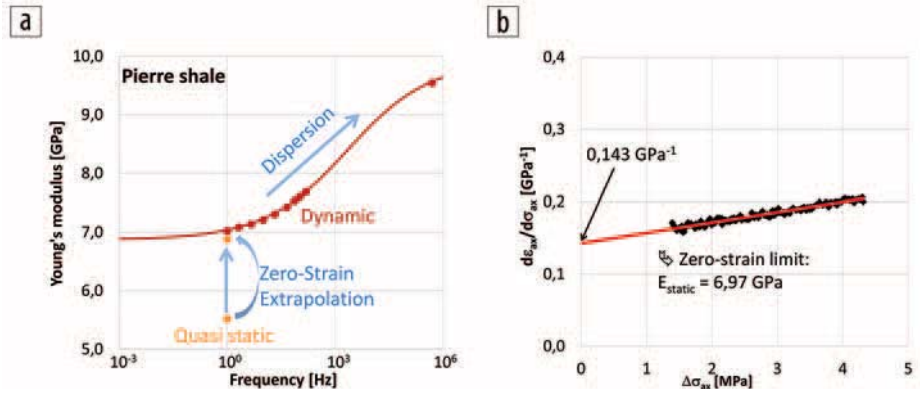

Figure 2. Seismic dispersion of Pierre shale. (a) Dynamic Young's modulus perpendicular to bedding (at σ_{ax} = 21 MPa, p_{conf} = 19.5 MPa, and p_f = 2 MPa), as well as quasistatic Young's modulus obtained from undrained triaxial unloading (starting at σ_{ax} = 26 MPa, p_{conf} = 17 MPa, and p_f = 2 MPa) and the zero-strain limit of the static Young's modulus. The strain amplitude for dynamic measurements was ≤ 1 μstrain. (b) Tangential slope of the stress-strain curve measured during triaxial unloading. A linear fit to the data allows for extrapolation to zero stress/strain.

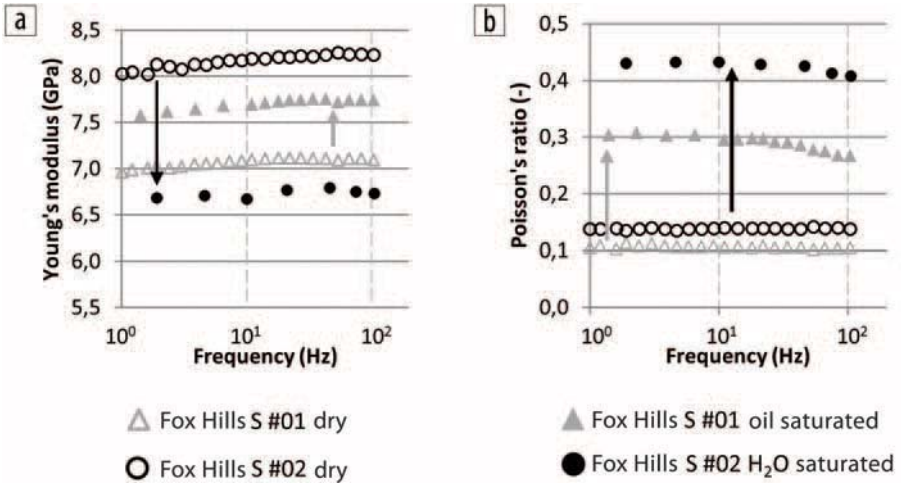

Figure 3. (a) Young's modulus and (b) Poisson's ratio as a function of frequency for dry, water-saturated, and oil-saturated Fox Hill sandstone.

Rock softening is observed when saturating sample no. 2 with water: Young's modulus decreases by about 15%, and Poisson's ratio strongly increases to values > 0.4. Szewczyk et al. (personal communication, 2016) made similar observations in shale. The dispersion in Young's modulus and Poisson's ratio of the sandstone at seismic frequencies is relatively small for both oil- and water-saturated samples. The dispersion seen in water-saturated shale, on the other hand, was much larger.

Shales: Stress dependence of velocities. Stress sensitivity of velocities is, among others, of importance for the quantitative interpretation of time-lapse seismic (4D seismic) (Hatchell and Bourne, 2005; Røste et al., 2015). Since velocity

measurements in the laboratory are usually done at frequencies > 100 kHz, while seismic measurements are done around 10–100 Hz, it is important to know if the stress sensitivities of velocities are frequency dependent.

In Figure 4, we show stress sensitivities of V_P and V_S measured with Mancos shale at both seismic and ultrasonic frequencies (as-received outcrop shale, with a water saturation corresponding to a relative humidity of 86%; Szewczyk et al., personal communication, 2016). The experiments have been carried out in the new low-frequency apparatus under different confining stresses and an additional axial stress of 2 MPa. (The low-frequency measurements require a finite deviatoric stress.) Since Mancos shale has been found to exhibit transversely isotropic (TI) symmetry , measurements have been carried out with three differently oriented cylindrical samples, with angles between sample axis and bedding of 0°, 45°, and 90°, respectively, in order to obtain all five independent stiffness parameters for both seismic and ultrasonic frequencies.

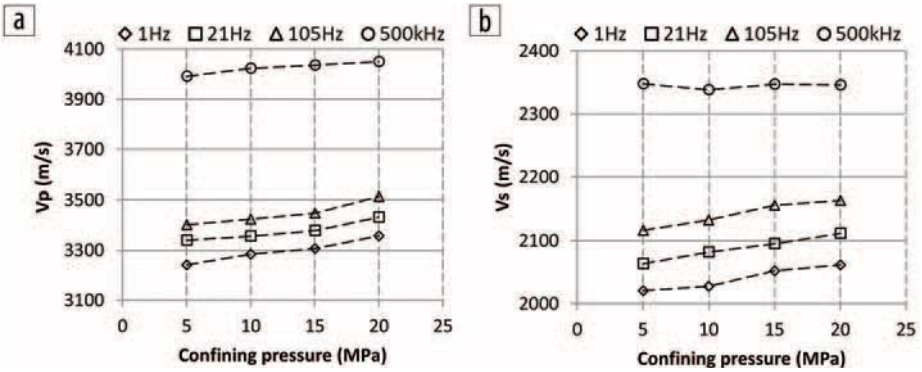

Figure 4. Stress dependence of compressional and shear-wave velocities, V_P and V_S, of Mancos shale as a function of confining stress for seismic and ultrasonic frequencies.

In Figure 4, V_P and V_S perpendicular to bedding are plotted as a function of confining stress for 1 Hz, 21 Hz, 105 Hz, and 500 kHz. It is obvious that both V_P and V_S exhibit significant dispersion. Between 1 Hz and 500 kHz, V_P and V_S increase by more than 20% and 15%, respectively. It is also apparent that the stress sensitivity is higher at seismic frequencies, in particular for V_S where nearly no variation with stress is observed at ultrasonic frequencies. At seismic frequencies, stress sensitivities amount to $\Delta V_P/V_P/p_{conf} \approx 2{\cdot}10\text{-}3\text{MPa-}1$ and $\Delta V_S/V_S/p_{conf} \approx 1.6{\cdot}10^{-3}\text{MPa}^{-1}$. At ultrasonic frequencies, the stress sensitivities are $\Delta V_P/V_P/p_{conf} \approx 1.0{\cdot}10^{-3}$ MPa^{-1} and $\Delta V_S/V_S/p_{conf} \approx$ -0.6 MPa^{-1}. It should be noted that there might be a significant error in the seismic V_P and V_S values, as they were derived from Young's moduli and Poisson's ratios measured with three different samples. Further studies are needed to verify the enhanced stress sensitivity at seismic frequencies.

Notice that previous experiments on Mancos Shale have showed significant dispersion (Suarez-Rivera et al., 2001) as well as no dispersion (Sarker and Batzle, 2010). In the former case, the specimens were partially water-saturated (like here), whereas in the latter case, they were fully saturated with decane. Thus, the level of saturation (Szewczyk et al., personal communication, 2016) as well the saturating fluid may impact the dispersion amount.

Conclusions

The experiments presented here have shown examples of dispersion in sand, sandstone, and shales. Observations are either direct through low-frequency (1–100 Hz) and ultrasonic (100–500 kHz) measurements, or indirect by interpretation of ultrasonic or standard static rock mechanical test data. The examples provide evidence that Biot dispersion is the main mechanism in clean unconsolidated sand. A consequence of this dispersion is that the shear modulus of dry and saturated sand is different, and that the Gassmann equation underestimates the observed dispersion. Interestingly, P- and S-wave dispersion shows opposite dependence on stress. Water-saturated Pierre Shale shows much stronger dispersion, in agreement with several observations in the literature. For the case of Pierre Shale, it is seen that the stress dependence for both P- and S-waves is larger in the seismic than in the ultrasonic frequency band. Shales are known to be softened by water, and a similar observation is made with Fox Hill sandstone, which can probably be explained by the presence of clay minerals.

This work is not complete, and several of the features described above are or will be the topic of further research. The main message we wish to communicate here is the continued need for frequency-dependent rock-physics laboratory experiments in order to assess the possible impact of dispersion on field data analysis. TLE

Acknowledgments

The authors wish to acknowledge partial financial support from The Research Council of Norway and industrial partners through the ROSE Program at NTNU, through the KPN-project "Shale Rock Physics: Improved seismic monitoring for increased recovery" at SINTEF Petroleum Research, and through the FME-project BIGCCS at SINTEF and NTNU. We are particularly grateful for help from and stimulating discussions with Audun Bakk and Jørn Stenebråten at SINTEF, and Manika Prasad at Colorado School of Mines.

Corresponding author: andreas.bauer@sintef.no

References

Adam, L., M. Batzle, and I. Brevik, 2006, Gassmann's fluid substitution and shear modulus variability in carbonates at laboratory seismic and ultrasonic frequencies: Geophysics, **71**, no. 6, F173–F183, http://dx.doi.org/10.1190/1.2358494.

Batzle, M. L., D.-H. Han, and R. Hofmann, 2006, Fluid mobility and frequency-dependent seismic velocity — Direct measurements: Geophysics, **71**, no. 1, N1–N9, http://dx.doi.org/10.1190/1.2159053.

Bhuiyan, M. H., and R. M. Holt, 2016, Variation of shear and compressional wave modulus upon saturation for pure pre-compacted sands: Geophysical Journal International, http://dx.doi.org/10.1093/gji/ggw156.

Biot, M. A., 1956, Theory of propagation of elastic waves in a fluid-saturated porous solid: II — Higher frequency range: The Journal

of the Acoustical Society of America, **28**, no. 2, 179–191, http://dx.doi.org/10.1121/1.1908241.
Duranti, L., R. Ewy, and R. Hofmann, 2005, Dispersive and attenuative nature of shales: Multiscale and multifrequency observations: 75th Annual International Meeting, SEG, Expanded Abstracts, 1577–1580, http://dx.doi.org/10.1190/1.2147994.
Fjær, E., A. Stroisz, and R. M. Holt, 2013, Elastic dispersion derived from a combination of static and dynamic measurements: Rock Mechanics and Rock Engineering, **46**, no. 3, 611–618, http://dx.doi.org/10.1007/s00603-013-0385-8.
Hatchell, P., and S. Bourne, 2005, Rocks under strain: Strain-induced time-lapse shifts are observed for depleting reservoirs: The Leading Edge, **24**, no. 12, 1222–1225, http://dx.doi.org/10.1190/1.2149624.
Johnson, D. L., and T. J. Plona, 1982, Acoustic slow waves and the consolidation transition: The Journal of the Acoustical Society of America, **72**, no. 2, 556–565, http://dx.doi.org/10.1121/1.388036.
Khazanehdari, J., and J. Sothcott, 2003, Variation in dynamic elastic shear modulus of sandstone upon fluid saturation and substitution: Geophysics, **68**, no. 2, 472–481, http://dx.doi.org/10.1190/1.1567213.
Mavko, G., and D. Jizba, 1994, The relation between seismic P- and S-wave velocity dispersion in saturated rocks: Geophysics, **59**, no. 1, 87–92, http://dx.doi.org/10.1190/1.1443537.
Müller, T. M., B. Gurevich, and M. Lebedev, 2010, Seismic wave attenuation and dispersion resulting from wave-induced flow in porous rocks — A review: Geophysics, **75**, no. 5, 75A147–75A164, http://dx.doi.org/10.1190/1.3463417.
Nakagawa, S., and T. Kneafsey, 2010, Split Hopkinson resonant bar test and its application for seismic property characterization of geological media: ARMA, paper ARMA-10-491.
O'Connell, R. J., and B. Budiansky, 1977, Viscoelastic properties of fluid-saturated cracked solids: Journal of Geophysical Research, **82**, no. 36, 5719–5735, http://dx.doi.org/10.1029/JB082i036p05719.
Røste, T., O. P. Dybvik, and O. K. Søreide, 2015, Overburden 4D time shifts induced by reservoir compaction at Snorre Field: The Leading Edge, **34**, no. 11, 1366–1374, http://dx.doi.org/10.1190/tle34111366.1.
Sarker, R., and M. Batzle, 2010, Anisotropic elastic moduli of the Mancos B Shale — An experimental study: 80th Annual International Meeting, SEG, Expanded Abstracts, 2600–2605, http://dx.doi.org/10.1190/1.3513381.
Spencer Jr., J. W., 1981, Stress relaxation at low frequencies in fluid saturated rocks: Attenuation and modulus dispersion: Journal of Geophysical Research, **86**, B3, 1803–1812, http://dx.doi.org/10.1029/JB086iB03p01803.
Suarez-Rivera, R., S. Willson, S. Nakagawa, O. M. Nes, and L. Zhuping, 2001, Frequency scaling for evaluation of shale and mudstone properties from acoustic velocities: Presented at the 2001 Fall Meeting, AGU.
Xu, S., and R. E. White, 1995, A new velocity model for clay-sand mixtures: Geophysical Prospecting, **43**, no. 1, 91–118, http://dx.doi.org/10.1111/j.1365-2478.1995.tb00126.x.